Transition energies and oscillator strengths for the intrashell and intershell transitions of the C-like ions in a thermodynamic equilibrium plasma environment

Chensheng Wu [1,2] Yong Wu,[1] Jun Yan,[1] T. N. Chang [3] and Xiang Gao [2,4,*]

[1]*Institute for Applied Physics and Computational Mathematics, Beijing 100088, China*
[2]*Beijing Computational Science Research Center, Beijing 100193, China*
[3]*Department of Physics, University of Southern California, Los Angeles, California 90089-0484, USA*
[4]*Institute for Theoretical Physics, Vienna University of Technology, A-1040 Vienna, Austria*

We present a theoretical study of the transition energies ω and the oscillator strengths gf for the C-like ions (with Z from 14–36) subject to plasma environment for atomic transitions, which meet the spatial and temporal criteria of the Debye-Hückel (DH) approximation. Two strong dipole-allowed transitions, viz., the intrashell transition $2s2p^3\ ^3D_1 \rightarrow 2s^22p^2\ ^3P_0$, and the intershell transition $2s^22p3d\ ^3D_1 \rightarrow 2s^22p^2\ ^3P_0$ are investigated in detail. We found that both ω and gf increase for the intrashell transition under the Debye-Hückel screening potential V_{DH} in terms of the Debye length D, which is linked to the ratio between the plasma density N_e and its temperature kT. In contrast, both ω and gf decrease for the intershell transition. Our theoretically estimated data have led to a general scaling feature for the change in ω of both intershell and intrashell transitions for ions with different nuclear charge Z. A similar general feature for the change in gf is also found for the intrashell transition. However, due to the change of the electron correlations between electrons in different shells with respect to the relativistic spin-orbit interaction as Z varies, the variation of gf subject to the surrounding plasma is more complicated for the intershell transition. The results presented in this work may facilitate the plasma diagnostic to determine the plasma temperature and density for the astrophysical objects and the controlled fusion facilities.

I. INTRODUCTION

Precision data, such as the transition energies ω and the oscillator strengths gf for the atomic or molecular processes, subject to the surrounding plasma environment in their ionic forms, are of great importance to the numerical modeling of the temporal-spatial evolution for systems in many of the astrophysical objects or in the energy related controlled fusion facilities [1–5]. Reliable atomic and molecular data are also important in the diagnostic analysis of the plasma parameters, such as the density and the temperature of plasma [6,7]. To fully understand the atomic processes subject to the surrounding plasma environment, one would need to include in the theoretical study the many-body interactions both between the atomic electrons and also the long-range Coulomb interaction between the atomic electrons and all the positive and negative charges of the surrounding plasma. Based on various approximations, attempts have been carried out over the years with somewhat sophisticated models to investigate the atomic processes in plasma environment [6,8–19].

The Debye-Hückel (DH) approximation, based on the classical Maxwell-Boltzmann statistics for an electron-ion collisionless plasma, works best for a gas discharge plasma at relatively low density [20,21]. For a judicious application of the DH approximation (i.e., a phenomenological model) to the atomic processes subject to surrounding charged-neutral plasma, there are two key criteria that need to be considered. First, spatially, the atomic processes should involve atomic orbitals, which are affected only marginally by the surrounding plasma, i.e., the DH approximation works only for transitions involving relatively small quantum number n such as the experimentally observed α and β emission lines of the H-like and He-like ions, which retain most of their atomic characteristic [22–27]. Second, temporally, the time scale of the atomic process (e.g., lifetime) has to be considerably different (either much greater or much smaller) from the correlation time (i.e., the inverse of the plasma frequency) of the surrounding plasma [8,9]. In fact, it is this temporal criterion that leads to our conclusion that the DH approximation would work for the H-like and He-like ions when the nuclear charge is between 6 and 18 or greater than 50. More detailed discussions on these two key criteria were given elsewhere [28–32].

In addition, the DH model depends on two key parameters. The first one is the radius of the Debye sphere A, which is an *ad hoc* parameter that separates the plasma induced Debye potential V_{DH} outside the Debye sphere and the slightly modified close-in region where the atomic characteristic dominates. We should point out that the Debye radius A employed in the application of the DH model in our study is different from the mean minimum radius of the ion sphere R_0 defined in various ion sphere approximations. More detailed discussion will be presented in Sec. III. The second one is the Debye length D, which is expressed in the units of Bohr radius a_0

in terms of the ratio of the temperature $k_b T$ and the electron density N_e (in the units of eV and 10^{22} cm^{-3}, respectively) of the surrounding plasma as

$$D = 1.4048 \times \sqrt{\frac{k_b T}{N_e}}. \tag{1}$$

In the limit when N_e equals to zero for the plasma-free environment, D goes to infinity. The Debye potential V_{DH} for the atomic electron can be expressed as [28,32–34]

$$V_{\text{DH}}(r_i) = \begin{cases} V_i(r_i) = -Z\left(\frac{1}{r_i} - \frac{1}{D+A}\right), & r_i \leqslant A, \\ V_o(r_i) = -Z\left(\frac{De^{A/D}}{D+A}\right)\frac{e^{-r_i/D}}{r_i}, & r_i > A. \end{cases} \tag{2}$$

We note that the atomic units are used throughout this paper if not otherwise specified. The presence of the $e^{-r/D}$ screening term in V_{DH} makes it less attractive than the plasma-free Coulomb potential $-Z/r$ due to the nucleus. When $A = 0$, V_{DH} takes the form of the screened Coulomb potential $-(Z/r)e^{-r/D}$, similar to the Yukawa potential in nuclear physics.

The DH model, due to its simplicity, has been extensively applied to investigate the influence of the plasma environment to the atomic processes [35–46]. We should point out, however, that many of these recent applications have included the Debye screening in the two-particle Coulomb interaction between atomic electrons. Theoretically, the Debye potential V_{DH} is derived from the Gauss theorem by assuming an infinitely heavy force center (such as the heavy nucleus with charge Z located at $r = 0$) in the presence of the fast free-moving plasma electrons with relatively high mobility. Since one could not assume a substantial presence of the plasma ions, with their low mobility, between the relatively fast-moving nonstationary atomic electrons, there is no theoretical justification to include the Debye screening in the two-body Coulomb potential at all. Such application could lead to results from the theoretical calculation against the physical intuition. One such unphysical example is the result that suggests the only known loosely bound H$^-$ state would stay bound in the presence of very strong surrounding plasma based on a high-precision rigorous calculation with the Debye screen included in the Coulomb potential between the two loosely bound electrons [45,46].

To demonstrate the feasibility of applying the DH approximation to the appropriate atomic processes, which meets the two criteria discussed above, we have carried out recently detailed studies of the α-emission lines of the H-like and He-like ions subject to surrounding plasma [29–32]. Our calculated red shifts in transition energy are in agreement both with the experimentally observed data [26,27,32] as well as the results from more elaborate simulations based on the quantum mechanical approaches [8–10,19]. We also note that whereas the recent calculated red shifts $\Delta\omega$ from the analytical IS (ion sphere) model for the α emission of the He-like Al ion are in agreement with the picosecond time-resolved measurement [26], its estimated redshifts at fixed temperature are substantially larger than the data from the high-resolution satellite lines-free measurement of the β line of He-like Cl ions [27]. Furthermore, shortly after the results of the He-like Cl ions experiment were reported, a good agreement in the calculated

red shifts with the observed data was reported by applying an average atom ion sphere (AIS) model with the energy terms evaluated by the relativistic multiconfiguration calculation [47]. However, the subsequent application of this AIS model to the α emission of the He-like Al ions has led to the red shifts substantially smaller than the earlier experimentally observed data [48].

Our studies have also led to a simple scaling feature for the red shifts of the transition energy and the oscillator strength as functions of a reduced Debye length $\lambda_D = Z_{\text{eff}}D$, defined as the product of the Debye length D and the effective nuclear charge Z_{eff} experienced by the atomic electrons [32]. For example, the ratio between the shifts in the transition energy $\Delta\omega$ and the plasma-free transition energy ω_0, viz., $R_\omega = \Delta\omega/\omega_0$, could be expressed by a simple polynomial in terms of the reduced Debye length λ_D [32] for all ions with applicable nuclear charge Z. Indeed, our calculations with the nonrelativistic and the relativistic multiconfiguration calculations have confirmed such general scaling feature [31,32]. By introducing this new parameter λ_D, we are able to focus our application of this slightly modified DH approximation for the general features of the atomic transition data that could be extended to all applicable ions in a single theoretical study.

Along this line, we have also studied the 3C and 3D lines of the Ne-like ions under the influence of the surrounding plasma [49]. For the dipole-allowed 3C line, the red shifts of the transition energy and the oscillator strength follow the similar scaling feature as those for the α lines of the H-like and He-like ions [29–32]. However, for the dipole-forbidden 3D line, due to the interplay between the relativistic spin-orbit interaction and the plasma screening effects, the simple scaling feature, which works well for the dipole-allowed transitions fails to follow. It is then interesting to investigate if any other atomic dynamics would influence such scaling feature. One of the main objectives of this paper is to present the results of our continuous investigation to other atomic processes where the combined effect of the electron-electron interaction and the relativistic spin-orbit interaction may alter the simple scaling feature we discussed earlier. More specifically, we have extended our study to the process beyond the intershell transitions studied earlier to include the intrashell transitions for the C-like ions, viz., focusing on two strong dipole allowed transitions, (i) the $2s^2 2p3d \; ^3D_1 \rightarrow 2s^2 2p^2 \; ^3P_0$ intershell transition (denoted as transition T1) and (ii) the $2s2p^3 \; ^3D_1 \rightarrow 2s^2 2p^2 \; ^3P_0$ intrashell transition (denoted as transition T2). We note that although there are some systematical studies on the atomic structure of C-like ions (e.g., Ref. [50]), the studies on the plasma effects to the C-like ions are scarce.

In Sec. II, we briefly outline the theoretical procedure leading to the full relativistic multiconfiguration calculation following our more detailed discussion elsewhere [49]. Our numerical results on the variation of the shifts of the transition energy $\Delta\omega$ and the oscillator strength gf as functions of the reduced Debye length are presented in Secs. III and Sec. IV, respectively. In addition to the scaling features in the ratio $R_\omega = \Delta\omega/\omega_0$ and the change in the oscillator strength gf as indicated earlier, we will focus our discussion on the interplay between the electron-electron correlation and the spin-dependent interaction and how it affects the intershell

process such as the transition T1. Finally, we will discuss briefly in Sec. V the implications of the works presented in this paper, and make a conclusion in Sec. VI.

II. THEORETICAL METHODS

For a relativistic calculation of a N-electron ions with nuclear charge Z subject to the surrounding plasma, the N-electron Hamiltonian $\hat{H}_{\mathrm{DH}}$ can be expressed as,

$$\hat{H}_{\mathrm{DH}} = \hat{H}_{\mathrm{DC}} + \sum_{i=1}^{N}\left[\frac{Z}{r_i} + V_{\mathrm{DH}}(r_i)\right], \quad (3)$$

where $\hat{H}_{\mathrm{DC}}$ is the well-known Dirac-Coulomb Hamiltonian in the absence of the plasma environment [51].

The atomic state functions (ASFs) $|\Gamma PJM\rangle$ (with P the parity, J the total angular momentum, M the magnetic quantum number, and Γ represents all other information to define the ASF uniquely) can be calculated by solving the following equation:

$$\hat{H}_{\mathrm{DH}}|\Gamma PJM\rangle = E_{\mathrm{DH}}^{\Gamma}|\Gamma PJM\rangle. \quad (4)$$

The ASFs are N-electron eigenstate wave functions, which are the linear combinations of the configuration state functions (CSFs) with the same P, J, and M, namely,

$$|\Gamma PJM\rangle = \sum_{i=1}^{n_e} C_i^{\Gamma}|\gamma_i PJM\rangle, \quad (5)$$

where C_i^{Γ} is the expansion coefficient and γ_i represents all other information to define the CSF uniquely. The CSFs, $|\gamma_i PJM\rangle$, which form a basis set for an N-electron atomic system in Hilbert space, are linear combinations of the Slater determinants of the atomic orbital wave functions (AOs). By applying the variational method to solve Eq. (4), one can obtain the mixing coefficients as well as the AOs self-consistently. This is known as the multiconfiguration self-consistent field method (MCSCF) [51,52]. Our calculations were carried out by using a revised multiconfiguration Dirac-Fock (MCDF) approach based on the quasicomplete basis scheme in order to take the electron correlations into account adequately [53–55]. Briefly, the basis satisfies the desired accuracy of calculations is called as a quasicomplete basis, which consists of spectroscopic AOs (with $n - l - 1$ fixed nodes) and pseudo-AOs (without fixed nodes). Both the spectroscopic and the pseudo-AOs can be specified by the principal quantum number n, the orbital angular momentum l and the total angular momentum j. The number of spectroscopic orbitals depends on the requirement of specific physical problem, i.e., degrees of excitations of target ions, while the number of pseudo-orbitals is determined by the desired accuracies. Such quasicomplete basis scheme is adopted to optimize the atomic orbitals (AOs) using the GRASP-JT version based on the earlier GRASP2K code [52]. Details of such application has been presented elsewhere [53–55]. More specifically, a two-step calculation procedure is adopted in the present work.

In the first step, we obtain the AOs based on the Dirac-Coulomb (DC) Hamiltonian $\hat{H}_{\mathrm{DC}}$ from Eq. (3), in the absence of the external plasma. AOs for ground and excited states are optimized separately to provide more flexibility for the later DH calculations. For example, in the calculation of $2s^2 2p3d\ ^3D_1$ state, spectroscopic AOs with $n = 1$, 2, and 3 are optimized to minimize all relevant 26 energy levels by MCSCF iterations, which form the zeroth level basis. We note that under the influence of the surrounding plasma, the interaction between electrons and nucleus decrease, which leads to the expansion of the AOs. To consider the possible expansion of AOs in plasma environments, we further added the spectroscopic AOs with $n = 4$, where all levels from the reference configurations $2s^2 2p3s$, $2s^2 2p3p$, $2s^2 2p3d$, $2s^2 2p4s$, $2s^2 2p4p$, $2s^2 2p4d$, and $2s^2 2p4f$ are minimized to obtain the first level basis. With $n = 1$, 2, 3, 4 spectroscopic AOs fixed, the pseudo-AOs, which are used to deal with the correlation between electrons are optimized with further MCSCF iterations to form the higher-level basis. The additional configuration state functions (CSFs) adopted in the optimization are generated by all single and double excitations from the $2s^2 2p3s$ and $2s^2 2p3d$ reference configurations. By adding more and more AOs and further expanding the level basis, finally we obtain the quasicomplete basis to achieve the numerical accuracy we need. In the present calculation, we have included in the quasicomplete basis with $n_{\max} = 6$ for the $2s^2 2p3d\ ^3D_1$ excited state. Similarly, for the $2s^2 2p^2\ ^3P_0$ and $2s2p^3\ ^3D_0$ states, we have included in the quasicomplete basis with spectroscopic AOs to $n = 3$, and $n_{\max} = 5$.

In the second step, the plasma effect is included by the configuration interaction (CI) calculation based on the optimized AOs [51,52]. The atomic state functions (ASFs) under the influence of the surrounding plasma are obtained in this step. With the calculated ASFs, the oscillator strength of transition between atomic states can be calculated. Under the dipole long wavelength approximation, the oscillator strength can be expressed as the product of the transition energy and the square of the transition matrix element in length gauge as,

$$g_\alpha f_{\alpha\beta} \sim \omega_{\alpha\beta} \cdot \left| \sum_{i,j} C_i^{\Gamma_\alpha} C_j^{\Gamma_\beta} \langle \gamma_i P_i J_i M_i|\hat{r}|\gamma_j P_j J_j M_j\rangle \right|^2, \quad (6)$$

where $\langle \gamma_i P_i J_i M_i|\hat{r}|\gamma_j P_j J_j M_j\rangle$ are the dipole transition matrix elements. By using the present quasicomplete basis scheme, we can examine the convergence of the calculation systematically. In the present calculation, the uncertainties for the strong transitions are estimated to be less than 0.2% for the excitation energies and 2% for the oscillator strengths. For such a small uncertainty, the results should be sufficient to offer an adequate qualitative feature on the variation of both the transition energy and the oscillator strength subject to external plasma environment.

III. TRANSITION ENERGY IN PLASMA

Table I shows that for different ions, our calculated plasma-free transition energies ω_0 are in good agreement with other theoretical and experimental results to within 0.2%. This close agreement indicates that the electron correlations are already taken into account adequately in our calculation. Based on the spatial and temporal criteria of the DH approximation [29–31,49], we investigate the intershell $2s^2 2p3d\ ^3D_1$-$2s^2 2p^2\ ^3P_0$ (viz., T1) transition and the intrashell

TABLE I. The calculated plasma-free transition energies ω_0 in unit of eV for a number of C-like ions in comparison with other theoretical and experimental results.

	Transition	ω_{Cal}[a]	ω_{Theory}[b]	ω_{Exp}[c]
Si	T1	224.070	224.012	224.183
	T2	36.289	36.215	36.258
Ar	T1	422.997	422.974	422.890
	T2	52.503	52.446	52.476
Ti	T1	684.172	684.177	684.270
	T2	71.958	71.914	71.924
Fe	T1	1009.032	1009.060	1009.000
	T2	96.354	96.303	96.300
Zn	T1	1399.523	1399.540	
	T2	127.304	127.279	127.230
Se	T1	1857.826	1857.840	
	T2	166.525	166.512	
Kr	T1	2113.197	2113.210	
	T2	189.816	189.820	189.720

[a]Present calculation.
[b]Reference [50].
[c]NIST [56].

$2s2p^3\ {}^3D_1$-$2s^22p^2\ {}^3P_0$ (viz., T2) transition under the plasma environment for different C-like ions with Z from 14–36 with the transition time scale at least one order of magnitude higher than the plasma correlation time. We have chosen in our calculation the radius of the Debye sphere A as the product of the average radius of $1s$ orbital of the C-like ions $\langle r_{1s}\rangle$ and a size parameter η, viz., $A = \eta\langle r_{1s}\rangle$. As we pointed out in Sec. I that to keep the atomic characteristic and simultaneously taking into account the surrounding plasma effects, the parameter A in our application of the DH approximation is assumed to be close to the size of the atomic orbitals involved. Hence, in the present calculation, three typical conditions with $\eta = 0, 1$, and 2 are calculated. The Debye length D, which should be much greater than A, starts from $2a_0$ for the lightest Si and a_0 for the heaviest Kr ions. On the other hand, the value of A defined as the mean minimum radius of the ion sphere R_0 in various ion sphere approximations is based on the assumption of the global charge neutrality in a spherical cavity, which is substantially greater than the average size of the atomic orbitals involved in the atomic processes being studied, i.e., the effect to the atomic process of the surrounding plasma may be greatly reduced. With the close agreements between the theoretically estimated energy shifts from our studies and the known independently observed measurements [23,26,27,32], it appears that assigning A as an *ad hoc* parameter is more preferable in the application of DH approximation.

Qualitatively, one immediate consequence of the less attractive Debye potential V_{DH} is that all the atomic levels will experience an uplifting in energy. As a result, the change in the transition energy for an atomic transition subject to surrounding plasma, either red shifted or blue shifted, depends on the decrease or increase of the difference in the relative energy shifts of the initial and final state of the transition. Although the percentage change of the orbital energy is larger for electron with larger principal quantum number n due to the stronger surrounding plasma effect, its small plasma-free

orbital energy actually makes the net energy change smaller than the one for the electron with smaller n. On the other hand, for electron in the orbitals with the same n, the change in energy is greater for the one with larger orbital angular momentum, again due to the stronger surrounding plasma. Following the quasihydrogenic approximation, for the C-like ions, the intershell transition T1 could be viewed as the transition of electron between the $3d$ and $2p$ orbitals. Based on the DH approximation, one expects the energy uplifting for the $3d$ orbital less than the one for $2p$ orbital. Therefore, a smaller transition energy ω subject to surrounding plasma is expected, i.e., leading to a red shift. In contrast, for the intrashell transition T2 with a $2p$ to $2s$ transition, a larger energy change is expected for the $2p$ orbital than the one for the $2s$ orbital, thus, leading to a blue shift in ω. Quantitatively, the major energy shift $\Delta\omega(D)$ subject to external plasma could be given approximately by the difference in energy corrections between the initial and final H-like orbitals due to the difference in Coulomb potential and the screened Coulomb potential, viz., $\Delta V_d(r, D) = Z/r(1 - e^{-r/D})$. For a transition from $n'l'$ orbital to nl orbital, this can be estimated by the difference of the expectation values of $\Delta_{n'l'} = \langle n'l'|\Delta V_d|n'l'\rangle$ and $\Delta_{nl} = \langle nl|\Delta V_d|nl\rangle$, or, given analytically by,

$$\Delta\omega_{n'l'-nl}(D) = \Delta_{n'l'}(D) - \Delta_{nl}(D)$$
$$= \frac{3(n^2 - n'^2) + l'(l'+1) - l(l+1)}{4D^2}$$
$$+ O(1/D^3). \tag{7}$$

From Eq. (7), it can be seen readily that the $3d$-$2p$ transition line would have a red shift, while the $2p$-$2s$ intrashell transition line would have a blue shift, and the leading term of both shifts is proportional to $1/D^2$ in the lowest-order approximation.

For the H-like ions, the plasma-free transition energy of the intershell transition is proportional to the square of the nuclear charge number Z. Combined with the red shift in terms of $1/D^2$ leading term discussed above, the ratio between the red shift subject to the surrounding plasma and the plasma-free transition energy, viz., $R_\omega = \Delta\omega/\omega_0$ should approximately vary as a function of $1/\lambda_D^2$ with the reduced Debye length $\lambda_D = ZD$ [29]. The feature $\omega_0 \sim Z^2$ does not hold strictly for the multielectron C-like ions. Nevertheless, when Z is much greater than the number of electrons N, the interaction between atomic electrons is relatively small comparing to the Coulomb interaction between nucleus and electrons, and the plasma-free ω_0 of the intershell transition may still vary approximately as Z_{eff}^2 where $Z_{eff} = Z - N$ is the effective nuclear charge. As a result, the ratio R_ω for the intershell transition could still be expressed approximately in terms of the inverse of the reduced Debye length, viz., $1/\lambda_D$, with the reduced Debye length $\lambda_D = Z_{eff}D$ when Z is sufficiently greater than N. But, it is more complicated for the intrashell $2p$-$2s$ transition since the nonrelativistic orbital energies are degenerate for the hydrogenlike atoms with the same n and the leading Z^2 terms cancel out. However, a closer look at the intrashell T2 transition, the relevant transition is in fact from the $2p_{3/2}$ to $2s_{1/2}$ orbitals with different j values due to the spin-orbit interaction, and the Z_{eff}^2 terms for the plasma-free
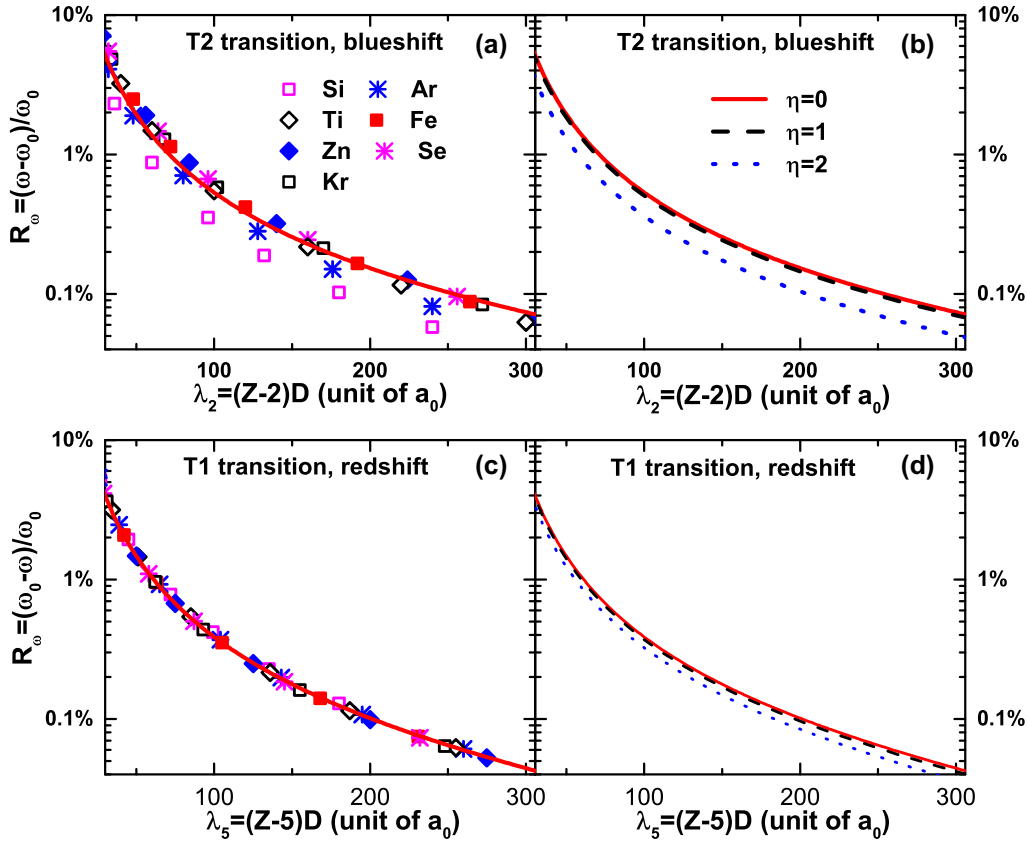
FIG. 1. The calculated and fitted ratios R_ω of the intrashell transitions T2 and the intershell transitions T1 as functions of the reduced Debye length λ_D with different $A = \eta\langle r_{1s}\rangle$ and the size parameter $\eta = 0$, 1, 2.

initial and final orbitals do not cancel out completely. As a result, one could still expect the ratio R_ω for the intrashell T2 transition between the blue shift and the plasma-free ω_0 varies with $1/\lambda_D$ for the C-like ions when Z is substantially greater than N and the electron correlations between the atomic electrons is less important.

Like our previous works on the α-emission lines for the H-like and He-like ions and the 3C and 3D lines for the Ne-like ions [29,31,49], our calculated ratio R_ω for the intershell transition for the C-like ions follows a similar general feature as a function of the reduced Debye length $1/\lambda_D$ for all ions, which follow the spatial and temporal criteria of the DH approximation. In fact, it is more convenient to fit numerically the ratio R_ω in terms of a simple polynomial expression,

$$R_\omega = \frac{|\Delta\omega|}{\omega_0} = \left\{ \begin{array}{ll} \frac{\omega_0 - \omega}{\omega_0}, & \text{red shift for T1} \\ \frac{\omega - \omega_0}{\omega_0}, & \text{blue shift for T2} \end{array} \right\}$$
$$= a_\omega + b_\omega/\lambda_D + c_\omega/\lambda_D^2. \qquad (8)$$

Note that, we define the ratios R_ω to be always positive for both red shift and blue shift of transitions in present work for convenience. This fitting expression takes into account the dominant contribution of the $1/\lambda_D^2$ term. The $1/\lambda_D$ term is used to represent mainly the contribution of electron correlations. One should also expect that the contribution from the fitting coefficient a_ω to the ratio R_ω is relatively small in comparison to the two other terms since, theoretically, R_ω should approach zero as λ_D goes to infinity. In other words,

effectively, a_ω represents the uncertainty of the estimated ratio R_ω in our theoretical calculation. We also expect that the coefficient c_ω is substantially greater than the other coefficient b_ω since the ratio varies approximately as $1/\lambda_D^2$ as we discussed earlier when the electron correlation and the relativistic interactions are relatively small. With $R_\omega(\lambda_D)$ given by Eq. (8), the shifts in excitation energy $\Delta\omega$ due to the surrounding plasma for a given pair of temperature and density could be estimated easily from the plasma-free ω_0 for ions with different Z, viz., $\Delta\omega = R_\omega(\lambda)\omega_0(Z)$. More details are given in Ref. [32].

Our calculated R_ω for a number of ions as the functions of $\lambda_2 = (Z - 2)D$ for the intrashell T2 transition and $\lambda_5 = (Z - 5)D$ for the intershell T1 transition with $\eta = 0$ are shown in Figs. 1(a) and 1(c). For the intrashell transition T2, only two $1s$ electrons contribute to the screening of the transition electrons from the nucleus and thus, $Z_{\text{eff}} = Z - 2$. For the intershell transitions T1, all five $n = 1$ and $n = 2$ electrons contribute to the screening and $Z_{\text{eff}} = Z - 5$. To simplify our discussion for the variation of R_ω as functions of the reduced Debye length λ_D and also taking into account the small deviation due to the relatively small contribution from the electron correlation as well as the spin-dependent interactions, we carry out a single least-square fit each for the transition T1 and T2, respectively, from a common data set composed of the calculated results for all C-like ions such as the ones shown in Figs. 1(a) and 1(c) for $\eta = 0$. Our fitted results with such a procedure are listed in Table II and also shown in Figs. 1(b) and 1(d) for T2 and T1, respectively, with $\eta = 0$, 1, and 2. As expected, the

TABLE II. The fitting coefficients for R_ω from Eq. (8).

R_ω	Transition	a_ω	b_ω	c_ω
$\eta = 0$	T1	-1.21×10^{-4}	0.054	34.44
	T2	-1.30×10^{-4}	0.12	42.79
$\eta = 1$	T1	-1.23×10^{-4}	0.053	32.89
	T2	-1.23×10^{-4}	0.11	40.70
$\eta = 2$	T1	-1.20×10^{-4}	0.049	28.71
	T2	-0.95×10^{-4}	0.085	28.49

fitted coefficients c_ω are much greater than the coefficients b_ω, indicating the relatively small contribution from the electron correlation and the relativistic interactions to the transition energy. Also, similar to the α-emission lines for the H-like and He-like ions, for the intershell transition T1, the fitted result pretty much reproduces the calculated data for all C-like ions shown in Fig. 1(c). For the intrashell transition T2, the calculated data for the low Z ions, such as Si^{8+} and Ar^{12+}, are slightly deviated from the fitted result due to the relatively large contribution from the electron correlation to the energy difference between the $2p$ and $2s$ orbitals as we pointed out earlier. Figure 1 also shows that the ratios R_ω for both T1 and T2 transitions vary more sensitively when η decreases from 2–1 than the decrease in η between 1 and 0 when the surrounding plasma impacts the atomic orbitals somewhat less for the smaller Debye sphere. With an improved experimental uncertainty in the recent extra-short-pulsed high-resolution experiments [26,27], together with our estimated data, one might be able to determine more precisely the size factor for our modified DH calculation.

IV. OSCILLATOR STRENGTH IN PLASMA

We will now turn our discussion to the oscillator strength $g_\alpha f_{\alpha\beta}$ for the transition from state α to state β given by Eq. (6) under the dipole long wavelength approximation in terms of the dipole matrix between the CSFs $|\gamma_i P_i J_i M_i\rangle$ and $|\gamma_j P_j J_j M_j\rangle$. Table III shows that our calculated plasma-free oscillator strengths are in good agreement with the results from Ref. [50] with the largest difference about 2% for the lightest C-like Si ion, indicating a reliable starting point for our study due to the plasma environment. For the intrashell $2p$-$2s$ T2 transition, it is not anticipated that the spin-dependent interactions might affect noticeably the oscillator strength as Z varies. Similar to the discussion on the transition energies, the ratios between the oscillator strengths variations subject to external plasma and their respective plasma free values can be expressed approximately in terms of the reduced Debye length λ_D by a similar expression,

$$R_{gf} = \frac{|\Delta gf(\lambda_D)|}{gf_0} = \begin{cases} \frac{gf_0 - gf(\lambda_D)}{gf_0}, & gf \text{ decrease for T1} \\ \frac{gf(\lambda_D) - gf_0}{gf_0}, & gf \text{ increase for T2} \end{cases}$$

$$= a_{gf} + b_{gf}/\lambda_D + c_{gf}/\lambda_D^2. \quad (9)$$

For the intershell $3d$-$2p$ T1 transition, the upper $2s^2 2p3d$, $^3D_1$ state is dominated by the $[2s^2 2p_{1/2} 3d_{3/2}]_1$ configuration when Z is much greater than N. For the lighter C-like ions, the contribution from other configurations, such as $[2s^2 2p_{3/2} 3d_{3/2}]_1$

TABLE III. The calculated plasma-free gf for the intershell transition T1 and the intrashell transition T2 in comparison with other theoretical results.

	Transition	gf_{Cal}[a]	gf_{Theory}[b]	Δgf_{Theory}[c]
Si	T1	1.035	1.032	0.3%
	T2	0.0794	0.0774	2%
Ar	T1	1.177	1.173	0.3%
	T2	0.0741	0.0733	1%
Ti	T1	1.244	1.239	0.4%
	T2	0.0776	0.0772	0.5%
Fe	T1	1.289	1.284	0.4%
	T2	0.0862	0.0860	0.2%
Zn	T1	1.325	1.321	0.3%
	T2	0.0968	0.0967	0.1%
Se	T1	1.355	1.352	0.2%
	T2	0.1078	0.1078	0.01%
Kr	T1	1.370	1.366	0.3%
	T2	0.1131	0.1131	0.02%

[a]Present calculation.
[b]Reference [50].
[c]Difference with Ref. [50].

and $[2s^2 2p_{3/2} 3d_{5/2}]_1$, may need to be included due to the spin-dependent interactions comparing to the dominating Z/r interaction. Figure 2 compares the contributions from various CSFs for the upper $2p3d$, $^3D_1$ state as functions of $\lambda_5 = (Z - 5)D$ with $\eta = 0$ for the C-like Si [Fig. 2(a)], Fe [Fig. 2(b)], and Kr [Fig. 2(c)] ions for weak, intermediate, and strong spin-orbit interaction, respectively. As we pointed out earlier, although $[2s^2 2p_{1/2} 3d_{3/2}]_1$ remains as the leading CSF for all ions, other CSFs may change noticeably as Z varies. For the C-like Si ion with the relatively weak spin-orbit interaction, all three main CSFs, $[2s^2 2p_{1/2} 3d_{3/2}]_1$, $[2s^2 2p_{3/2} 3d_{3/2}]_1$, and $[2s^2 2p_{3/2} 3d_{5/2}]_1$ originated from the nonrelativistic $2s^2 2p3d$ CSF, contribute more than 10% to its ASF. In contrast, the relatively strong spin-orbit interaction for the $2p$ orbital of the C-like Kr ion leads to a larger energy separation between the $2p_{1/2}$ and $2p_{3/2}$ orbitals and thus, most of the contribution to the oscillator strength comes from the dominating $[2s^2 2p_{1/2} 3d_{3/2}]_1$ CSF. For the C-like Fe ion with an intermediate spin-orbit interaction, contributions from different combination of CSFs are shown by Fig. 2(b). With such noticeable variation in the contributions to the oscillator strength from different combination of CFSs as Z varies, the scaling behavior for the intershell T1 transition may not follow the one given by Eq. (9).

Figure 3 presents our calculated R_{gf} of the T2 [Fig. 3(a)] and T1 [Fig. 3(c)] transitions for a number of C-like ions with the size factor $\eta = 0$. As expected, for the intrashell T2 transition, the ratio R_{gf} for all ions follow closely to the fitted ratio to Eq. (9) with the fitted coefficients listed in Table IV. In contrast, for the intershell T1 transition, our calculated R_{gf} for C-like Si ion is substantially larger than the one for the Kr ion due to the difference in spin-orbit interaction as discussed earlier. The fitted ratios R_{gf} with different size parameters for the T2 and T1 transitions are given by Figs. 3(b) and 3(d), respectively.
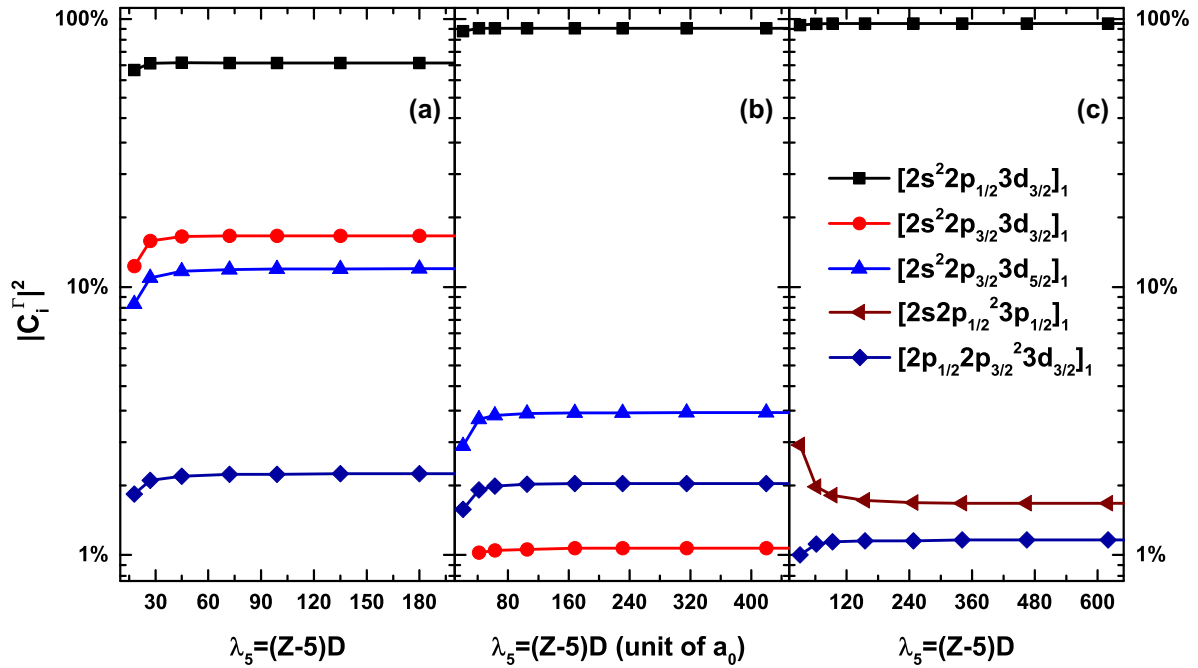
FIG. 2. The weights of the main CSFs in $2s^2 2p3d\ ^3D_1$ states in terms of the reduced Debye length $\lambda_D = Z_{\text{eff}}D$ for C-like (a) Si, (b) Fe, and (c) Kr ions.
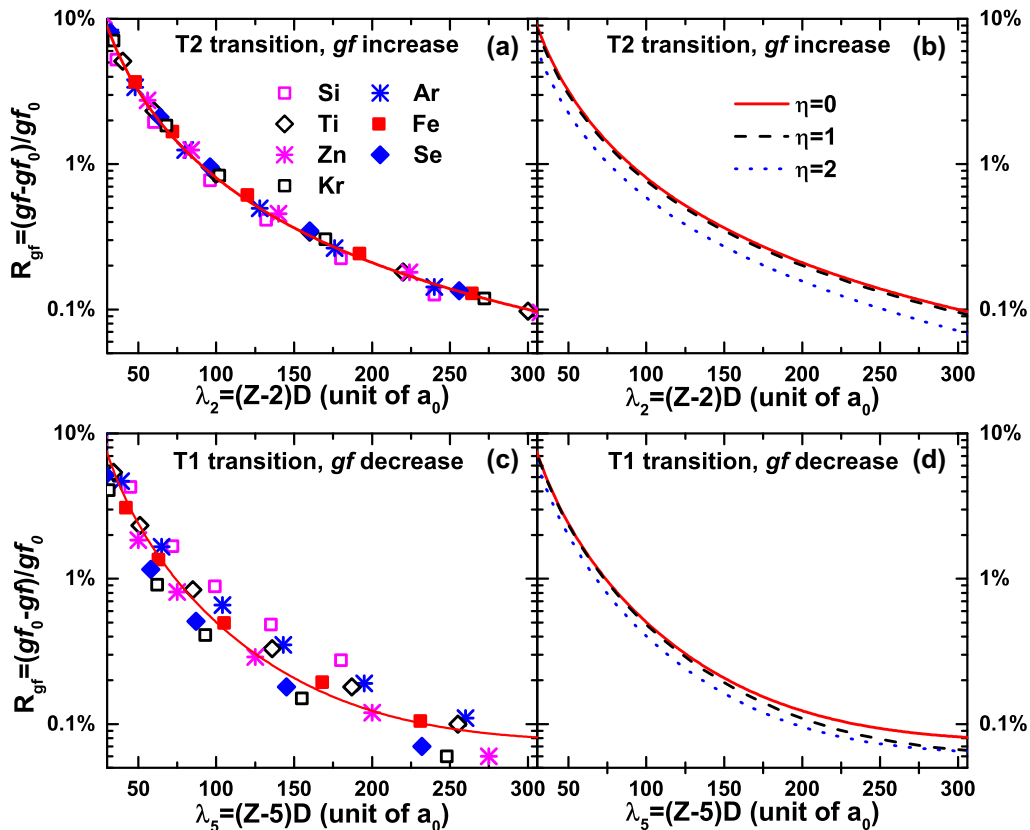

FIG. 3. The calculated and the fitted ratios R_{gf} of the intrashell transition T2 and the intershell transition T1 as functions of the reduced Debye length λ_D with different $A = \eta\langle r_{1s}\rangle$ and the size parameter $\eta = 0$, 1, and 2.

TABLE IV. The fitting coefficients for R_{gf} from Eq. (9).

R_{gf}	Transition	a_{gf}	b_{gf}	c_{gf}
$\eta = 0$	T1	0.0013	-0.38	76.15
	T2	1.26×10^{-4}	-0.0031	79.62
$\eta = 1$	T1	0.0010	-0.36	73.96
	T2	0.89×10^{-4}	0.0089	75.03
$\eta = 2$	T1	0.0011	-0.36	64.93
	T2	-0.96×10^{-4}	0.064	53.50

V. DISCUSSION

Experiments on the line shifts of the atomic transitions from H- and He-like ions in plasma environment in recent years have been carried out with plasma electron density from 10^{22} cm^{-3} to as high as 10^{24} cm^{-3} [23,26,27]. Figure 4 presents the variation of the energy shift ratios R_ω as the functions of density N_e up to 10^{24} cm^{-3} for the T1 and T2 transitions from the C-like Ar^{12+} ion at temperatures $k_b T = 400$, 800, and 1500 eV following the procedure discussed earlier based on Eq. (8) and the fitted coefficients listed in Table II. With the current experimental capability, the estimation of the transition energy shifts based on our modified DH model may help the choice of the plasma density N_e and the temperature $k_b T$ within the current experimental conditions for the potential measurements with the state-of-the-art energy resolution for the C-like ions.

As we discussed earlier in Sec. III, only one *ad hoc* parameter A subject to the spatial criterion is included in our application of the modified DH approximation to the energy shifts of the atomic emissions involving isolated low n states due to the surrounding plasma. With the close agreements between the known independently observed measurements [23,26,27,32] and our theoretically estimated energy shifts,

the application of the DH model offers a promising possibility to estimate the plasma effect to the atomic processes. Also, we would like to point out again that the parametrized expressions in terms of the reduced Debye length given by Eqs. (8)–(9), together with the fitted coefficients based on the numerical calculations listed in Tables II and IV, the shifts in excitation energy and the oscillator strength due to the surrounding plasma with a given pair of temperature and density could be estimated easily from the plasma-free ω_0 and gf_0 for ions with different Z, e.g., $\Delta\omega = R_\omega(\lambda)\omega_0(Z)$, either from the theoretical calculation or those listed from the NIST data [56]. The lack of *a priori* theoretical basis in defining the Debye radius A makes it necessary for additional experimental measurements with less uncertainty to determine more definitively its appropriate value to facilitate the theoretical calculation leading to more reliable atomic data.

VI. CONCLUSION

In summary, by applying the DH approximation, with its spatial and temporal criteria satisfied, we present a detailed theoretical study on the transition energies and the oscillator strengths of two dipole-allowed transitions for the C-like ions subject to plasma environment. The first one is the intershell transition T1 (viz., the $2s^2 2p3d\ ^3D_1 \rightarrow 2s^2 2p^2\ ^3P_0$ transition) and the second one is the intrashell transition T2 (viz., the $2s2p^3\ ^3D_1 \rightarrow 2s^2 2p^2\ ^3P_0$) with the nuclear charge Z from 14–36. For the intrashell transition T2, the ratio of the blue shift to its plasma-free transition energy and the increase of the oscillator strength due to the surrounding plasma follow the general scaling property similar to those for the α emission of the He-like and H-like ions shown in our earlier works [29–31]. Such scaling property could be understood qualitatively based on the simple quasihydrogenic approximation discussed earlier. For the intershell transition T1, the ratio of
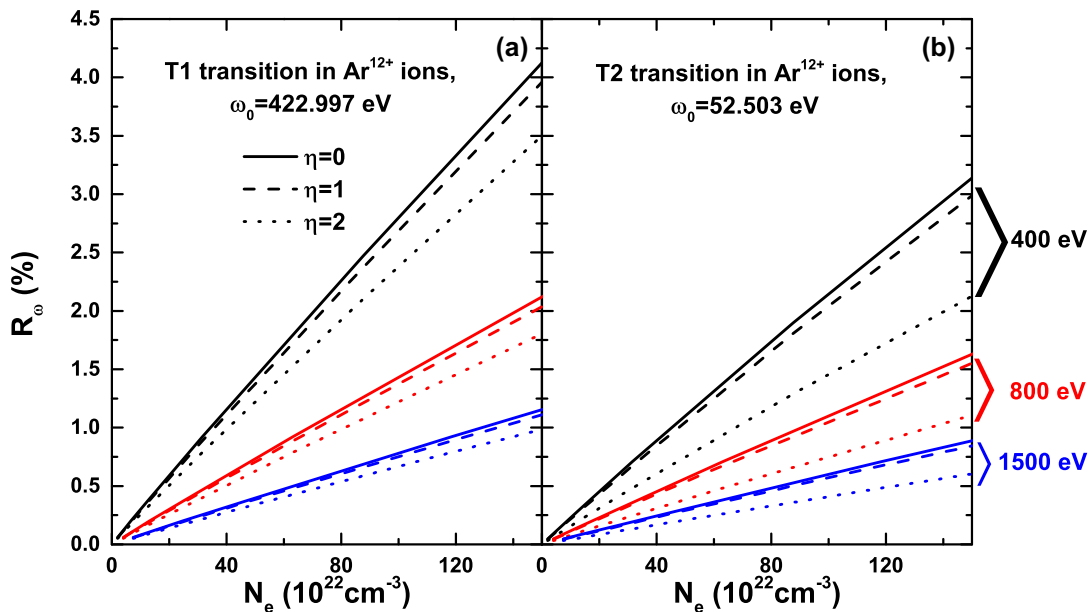

FIG. 4. The ratios R_ω of both T1 and T2 transitions from the C-like Ar^{12+} ion in terms of the plasma electron density N_e with temperature $k_b T = 400$ eV (black lines), 800 eV (red lines), and 1500 eV (blue lines).

the red shift and the plasma-free transition energy follows the similar scaling property. However, our study has shown, interestingly, the decrease in the oscillator strength fails to follow the scaling feature such as the one for the intrashell transition T2. Our detailed analysis suggests that this is due to the change of electron correlation with respect to the relativistic spin-orbit interaction as Z varies.

Finally, as shown by the present study, not all atomic transitions would follow the general scaling feature as we discussed. A detailed theoretical calculation for some of the atomic transition remains necessary to estimate the variation in the oscillator strength under the influence of surrounding plasma. A few percent change in the transition energy is certainly within the reach of the current experimental capability, although it may still be difficult to observe quantitatively the change in the oscillator strength. The theoretical calculations based on the DH approximation, such as the one we present for the C-like ions, may offer a viable choice of the plasma temperature and density in advance for the quantitative experimental measurement beyond the ones for H-like, He-like, and Ne-like ions.

[1] J. Tennyson, *Astronomical Spectroscopy: An Introduction to the Atomic and Molecular Physics of Astronomical Spectral* (PressImperial College, London, 2005).

[2] T. R. Kallman and P. Palmeri, Atomic data for x-ray astrophysics, Rev. Mod. Phys. **79**, 79 (2007).

[3] J. D. Lindl, P. Amendt, R. L. Berger, S. G. Glendinning, S. H. Glenzer, S. W. Haan, R. L. Kauffman, O. L. Landen, and L. J. Suter, The physics basis for ignition using indirect-drive targets on the national ignition facility, Phys. Plasmas **11**, 339 (2004).

[4] Allen H. Boozer, Physics of magnetically confined plasmas, Rev. Mod. Phys. **76**, 1071 (2005).

[5] R. E. H. Clark and D. H. Reiter, *Nuclear Fusion Research: Understanding Plasma-Surface Interactions* (Springer-Verlag, Berlin, 2005).

[6] S. Skupsky, X-ray line shift as a high-density diagnostic for laser-imploded plasmas, Phys. Rev. A **21**, 1316 (1980).

[7] H. R. Griem, *Principles of Plasma Spectroscopy*, Cambridge Monographs on Plasma Physics (Cambridge University Press, Cambridge, 1997).

[8] H. Nguyen, M. Koenig, D. Benredjem, M. Caby, and G. Coulaud, Atomic structure and polarization line shift in dense and hot plasmas, Phys. Rev. A **33**, 1279 (1986).

[9] M. Koenig, P. Malnoult, and H. Nguyen, Atomic structure and line broadening of he-like ions in hot and dense plasmas, Phys. Rev. A **38**, 2089 (1988).

[10] J. Davis and M. Blaha, Level shifts and inelastic electron scattering in dense plasmas, J. Quant. Spectrosc. Radiat. Transfer **27**, 307 (1982).

[11] S. H. Glenzer and R. Redmer, X-ray thomson scattering in high energy density plasmas, Rev. Mod. Phys. **81**, 1625 (2009).

[12] X.-F. Li, G. Jiang, H.-B. Wang, M. Wu, and Q. Sun, Transition energies, transition probabilities and weighted oscillator strengths of he-like al in hot and dense plasmas, Phys. Scr. **92**, 075401 (2017).

[13] M. Murillo, Dense plasmas, screened interactions, and atomic ionization, Phys. Rep. **302**, 1 (1998).

[14] S. Ichimaru, Strongly coupled plasmas: high-density classical plasmas and degenerate electron liquids, Rev. Mod. Phys. **54**, 1017 (1982).

[15] S.-K. Son, R. Thiele, Z. Jurek, B. Ziaja, and R. Santra, Quantum-Mechanical Calculation of Ionization-Potential Lowering in Dense Plasmas, Phys. Rev. X **4**, 031004 (2014).

[16] M. W. C. Dharma-wardana and F. C. Perrot, Density-functional theory of hydrogen plasmas, Phys. Rev. A **26**, 2096 (1982).

[17] G. Ecker and W. Kröll, Lowering of the ionization energy for a plasma in thermodynamic equilibrium, Phys. Fluids **6**, 62 (1963).

[18] J. C. Stewart and K. D. Jr. Pyatt, Lowering of ionization potentials in plasmas, Astrophys. J. **144**, 1203 (1966).

[19] F. Zhou, Y. Qu, J. Gao, Y. Ma, Y. Wu, and J. Wang, Atomic-state-dependent screening model for hot and warm dense plasmas, Commun. Phys. **4**, 148 (2021).

[20] P. Debye and E. Hückel, The theory of electrolytes I. The lowering of the freezing point and related occurrences, Phys. Z. **24**, 185 (1923).

[21] F. F. Chen, *Introduction to Plasma Physics and Controlled Fusion Plasma Physics* (Springer International Publishing, Switzerland, 2016).

[22] D. J. Hoarty, P. Allan, S. F. James, C. R. D. Brown, L. M. R. Hobbs, M. P. Hill, J. W. O. Harris, J. Morton, M. G. Brookes, R. Shepherd, J. Dunn, H. Chen, E. Von Marley, P. Beiersdorfer, H. K. Chung, R. W. Lee, G. Brown, and J. Emig, Observations of the Effect of Ionization-Potential Depression in Hot Dense Plasma, Phys. Rev. Lett. **110**, 265003 (2013).

[23] A. Saemann, K. Eidmann, I. E. Golovkin, R. C. Mancini, E. Andersson, E. Förster, and K. Witte, Isochoric Heating of Solid Aluminum by Ultrashort Laser Pulses Focused on a Tamped Target, Phys. Rev. Lett. **82**, 4843 (1999).

[24] M. Nantel, G. Ma, S. Gu, C. Y. Côté, J. Itatani, and D. Umstadter, Pressure Ionization and Line Merging in Strongly Coupled Plasmas Produced by 100-fs Laser Pulses, Phys. Rev. Lett. **80**, 4442 (1998).

[25] Y. Leng, J. Goldhar, H. R. Griem, and R. W. Lee, C-vi lyman line-profiles from 10-ps krf-laser-produced plasmas, Phys. Rev. E **52**, 4328 (1995).

[26] C. R. Stillman, P. M. Nilson, S. T. Ivancic, I. E. Golovkin, C. Mileham, I. A. Begishev, and D. H. Froula, Picosecond time-resolved measurements of dense plasma line shifts, Phys. Rev. E **95**, 063204 (2017).

[27] P. Beiersdorfer *et al.*, High-resolution measurements of cl^{15+} line shifts in hot, solid-density plasmas, Phys. Rev. A **100**, 012511 (2019).

[28] T. N. Chang and T. K. Fang, Atomic photoionization in a changing plasma environment, Phys. Rev. A **88**, 023406 (2013).

[29] T. N. Chang, T. K. Fang, and X. Gao, Redshift of the lyman-α emission line of h-like ions in a plasma environment, Phys. Rev. A **91**, 063422 (2015).

[30] T. K. Fang, C. S. Wu, X. Gao, and T. N. Chang, Variation of the oscillator strengths for the α emission lines of the one- and two-electrons ions in dense plasma, Phys. Plasmas **25**, 102116 (2018).

[31] T. K. Fang, C. S. Wu, X. Gao, and T. N. Chang, Redshift of the he α emission line of he-like ions under a plasma environment, Phys. Rev. A **96**, 052502 (2017).

[32] T. N. Chang, T. K. Fang, C. S. Wu, and X. Gao, Redshift of the isolated atomic emission line in dense plasma, Phys. Scr. **96**, 124012 (2021).

[33] H. Margenau and M. Lewis, Structure of spectral lines from plasmas, Rev. Mod. Phys. **31**, 569 (1959).

[34] C. A. Rouse, Finite electronic partition function from screened coulomb interactions, Phys. Rev. **163**, 62 (1967).

[35] P. K. Mukherjee, J. Karwowski, and G. H. F. Diercksen, On the influence of the debye screening on the spectra of two-electron atoms, Chem. Phys. Lett. **363**, 323 (2002).

[36] A. N. Sil and P. K. Mukherjee, Effect of debye plasma on the doubly excited states of highly stripped ions, Int. J. Quantum Chem. **102**, 1061 (2005).

[37] S. B. Zhang, J. G. Wang, and R. K. Janev, Electron-hydrogen-atom elastic and inelastic scattering with screened coulomb interaction around the $n=2$ excitation threshold, Phys. Rev. A **81**, 032707 (2010).

[38] S. B. Zhang, J. G. Wang, and R. K. Janev, Crossover of Feshbach Resonances to Shape-Type Resonances in Electron-Hydrogen Atom Excitation with a Screened Coulomb Interaction, Phys. Rev. Lett. **104**, 023203 (2010).

[39] Y. Y. Qi, Y. Wu, J. G. Wang, and Y. Z. Qu, The generalized oscillator strengths of hydrogenlike ions in debye plasmas, Phys. Plasmas **16**, 023502 (2009).

[40] S. T. Dai, A. Solovyova, and P. Winkler, Calculations of properties of screened he-like systems using correlated wave functions, Phys. Rev. E **64**, 016408 (2001).

[41] X. Lopez, C. Sarasola, and J. M. Ugalde, Transition energies and emission oscillator strengths of helium in model plasma environments, J. Phys. Chem. A **101**, 1804 (1997).

[42] S. Kar and Y. K. Ho, Oscillator strengths and polarizabilities of the hot-dense plasma-embedded helium atom, J. Quant. Spectrosc. Radiat. Transfer **109**, 445 (2008).

[43] S. Kar and Y. K. Ho, Photodetachment of the hydrogen negative ion in weakly coupled plasmas, Phys. Plasmas **15**, 013301 (2008).

[44] P. K. Shukla and B. Eliasson, Screening and wake potentials of a test charge in quantum plasmas, Phys. Lett. A **372**, 2897 (2008).

[45] S. Kar and Y. K. Ho, Electron affinity of the hydrogen atom and a resonance state of the hydrogen negative ion embedded in debye plasmas, New J. Phys. **7**, 141 (2005).

[46] A. Ghoshal and Y. K. Ho, Ground states and doubly excited resonance states of H$^-$ embedded in dense quantum plasmas, J. Phys. B: At. Mol. Opt. Phys. **42**, 175006 (2009).

[47] Z.-B. Chen, Calculation of the energies and oscillator strengths of Cl^{15+} in hot dense plasmas, J. Quant. Spectrosc. Radiat. Transfer **237**, 106615 (2019).

[48] Z.-B. Chen and K. Wang, Theoretical study on the line shifts of he-like al11+ ion immersed in a dense plasma, Radiat. Phys. Chem. **172**, 108816 (2020).

[49] C. Wu, S. Chen, T. N. Chang, and X. Gao, Variation of the transition energies and oscillator strengths for the 3c and 3d lines of the ne-like ions under plasma environment, J. Phys. B: At. Mol. Opt. Phys. **52**, 185004 (2019).

[50] K. Wang, D. F. Li, H. T. Liu, X. Y. Han, B. Duan, C. Y. Li, J. G. Li, X. L. Guo, C. Y. Chen, and J. Yan, Systematic calculations of energy levels and transition rates of c-like ions with $z=13$–36, Astrophys. J. Suppl. Series **215**, 26 (2014).

[51] I. P. Grant, *Relativistic Quantum Theory of Atoms and Molecules* (Springer-Verlag, New York, 2007).

[52] P. Jönsson, G. Gaigalas, J. Bieron, C. Froese Fischer, and I. P. Grant, New version: Grasp2k relativistic atomic structure package, Comput. Phys. Commun. **184**, 2197 (2013).

[53] X.-Y. Han, X. Gao, D.-L. Zeng, R. Jin, J. Yan, and J.-M. Li, Scaling law for transition probabilities in 2p^3 configuration from ls coupling to jj coupling, Phys. Rev. A **89**, 042514 (2014).

[54] X. Gao, X.-Y. Han, D.-L. Zeng, R. Jin, and J.-M. Li, Broken scaling laws of the transition probabilities from jj to ls coupling transitions, Phys. Lett. A **378**, 1514 (2014).

[55] X.-Y. Han, X. Gao, D.-L. Zeng, J. Yan, and J.-M. Li, Ratio of forbidden transition rates in the ground-state configuration of o ii, Phys. Rev. A **85**, 062506 (2012).

[56] A. Kramida, Y. Ralchenko, J. Reader, and NIST ASD Team, NIST Atomic Spectra Database (ver. 5.8), [Online]. Available at: https://physics.nist.gov/asd [2021, October 11] (National Institute of Standards and Technology, Gaithersburg, 2020).